Growth and characterization of transparent vanadium doped zinc oxide thin films by means of a spray pyrolysis process for TCO application

Ali Sadek Kadari[1] · Abdelkader Nebatti Ech-Chergui[2] · Brahim Aïssa[3] · Sanat Kumar Mukherjee[4] · Nourddine Benaioun[1] · Yahya Zakaria[3] · Atef Zekri[3] · Chellali Mohemed Reda[5] · Adjdir Mehdi[6] · Rahmani Rabea[1] · Kouider Driss-Khodja[1] · Bouhalouane Amrani[1]

Abstract

Aluminum doped zinc oxides show a high electrical conductivity owing to their high electron concentration in the conduction band, which significantly hinders the development of p-n junction due to the formation of degenerate states. To overcome this limitation, it is proposed to improve the electron mobility rather than the free electron concentration. For this specific aspect, vanadium appears to be one of the most suited alternatives as a doping element. In this work, we report on the preparation of ZnO and vanadium-doped ZnO thin films by spray pyrolysis process. Vanadium loads were varied from 0 to 4 at.% in the ZnO films and its effect on the structural, morphological, chemical, optical, and mechanical properties of the fabricated thin films was investigated through a bench of characterizations techniques, including X-ray diffraction (XRD), atomic force microscope (AFM), X-ray photoelectron spectroscope (XPS), time-of-flight secondary ion mass spectroscopy (TOF-SIMS), UV-Vis spectrophotometer, and digital Vickers microhardness tester. The obtained results demonstrate the successful formation of pristine ZnO films and V-doped ZnO, which were found to be polycrystalline with a hexagonal wurtzite crystal structure. According to the self-correlation function, AFM images reveal that the particle size increases with respect to the V-load. TOF-SIMS analyses confirm the constant distribution of Zn, O and V elements throughout the film thickness. Moreover, our films are found to be optically transparent in the 400–1200 nm range with associated band gaps energy ranging from 3.18 to 3.26 eV. Finally, mechanical measurements have been carried out using a conventional diamond-pyramidal-indenter Vickers test. The results confirmed that by increasing V concentration, the microhardness increases.

✉ Abdelkader Nebatti Ech-Chergui
abdelkader.nebatti@daad-alumni.de

1. Laboratory of Theory and Simulation of Materials, Faculty of Exact and Applied Sciences, University of Oran1, Ahmed Ben Bella, Oran, Algeria

2. Laboratory of Materials Sciences and Applications (LSMA), University of Ain-Temouchent Belhadj Bouchaib, Faculty of Sciences and Technology, Aïn Témouchent, Algeria

3. Qatar Environment and Energy Research Institute (QEERI), Hamad Bin Khalifa University (HBKU), Qatar Foundation, P.O. Box 5825, Doha, Qatar

4. Department of Applied Physics, Birla Institute of Technology, Mesra, India

5. Institute of Nanotechnology, Karlsruhe Institute of Technology, Hermann-von-Helmholtz-Platz 1, 76344 Eggenstein-Leopoldshafen, Germany

6. Laboratory of Applied Organic Synthesis, Faculty of Exact and Applied Sciences, University Oran1 Ahmed Ben Bella, P.O. Box 1524El M'Naouer, 31000 Oran, Algeria

Graphical abstract
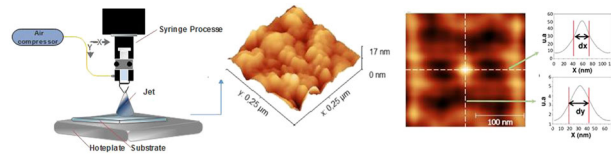
Keywords ZnO · V-doped ZnO · Spray pyrolysis · Surface roughness · Vickers microhardness

Highlights

- V-doped ZnO films successfully grown by the chemical spray pyrolysis technique.
- V-doped ZnO films are polycrystalline structure with a dominant (101) orientation.
- The surface roughness of the films is well controlled with respect to the V concentration and the average optical transmittance of all films was between 60% and 80%.
- TOF-SIMS analysis confirmed the presence of all the deposited elements over the surface and over the entire film thickness.
- The energy band gap varies from 3.18 and 3.26 eV w/r to V concentration.

1 Introduction

During the current decade, a focused scientific effort is put on the development of zinc oxide (ZnO) material for various applications. In fact, ZnO exhibits several significant characteristics because of its direct gap of 3.37 eV at room temperature, the high free-exciton binding energy of about 60 meV, and its excellent optical properties [1, 2]. The intrinsic n-type conductivity of ZnO is due to its stoichiometric deviations in the ZnO matrix, creating intrinsic shallow donor defects, particularly Zn interstitials (Zn_i) [3, 4]. ZnO is being considered as a prospective material in various transparent conductive oxides (TCO) applied for thin film transistors, light emitting devices (emitting in the UV region), flat panel displays, surface temperature sensor [5], and thin-film solar cells [6–9]. Intensive n-type doping, for example by group-III elements indium, gallium, aluminum, and boron substituting oxygen was used with an aim to attain superior electrical conductivities [10–12]. This field has seen a great deal of activity in order to reach conductivities approaching those of indium tin oxide, the dominant transparent electrode material today, where prospectively a shortage of In metal is expected [13, 14].

Usually, pristine ZnO and group-III elements doped ZnO thin films have been employed as transparent and conducting film. In particular, Al-doped ZnO (AZO) is the utmost significant material owing to its high electrical conductivity, and high optical transparency, its non-toxicity and the fact to be commercially available. It is also chemically stable in hydrogen plasma procedures, which are commonly employed to manufacture solar cells. In AZO, the higher conductivity is due to the higher electron concentration in the conduction band, which poses a significant difficulty for the development of p-n junction because of the formation of degenerate states [14]. ZnO thin films can be synthesized using a variety of techniques including, magnetron sputtering, e-beam evaporation, pulsed laser deposition [14–17], and chemical techniques, like sol–gel, chemical vapor deposition (CVD), metalorganic CVD, hydrothermal and spray pyrolysis [18–25]. Among these techniques, the spray pyrolysis is particularly indicated since it has been demonstrated to be a simple (non-vacuum), cost-effective, scalable, and efficient for large area applications [26, 27].

In this paper, the transition metal vanadium (V) was selected as the dopant, and the effects of its concentration on the characteristics of V-doped ZnO thin films were investigated, for application as TCO. The film growth, its structural, compositional, and optical properties were analyzed. the effect of dopant on the mechanical properties of a TCO is rarely examined. With the growing demand of flexible electronics, investigation on mechanical reliability of TCOs become crucial. This work addresses thus the variation in the mechanical properties assessed by Vickers tests of ZnO with V-doping and correlates them with time-of flight secondary ion mass spectroscopy (TOF-SIMS) techniques and AFM imaging. To the best of our knowledge, this is the first study of its kind, and we aim at proposing it as a reference in this matter. It is worth mentioning here that the current study did not focus on electrical properties of the materials due to the absence of the appropriate tool to do so. Hall effect measurements are to be systematically conducted to get a deep insight on the electronic properties' dependency as a function of the V doping level. Such in-depth and elaborate electrical analysis of these materials is planned as future work.
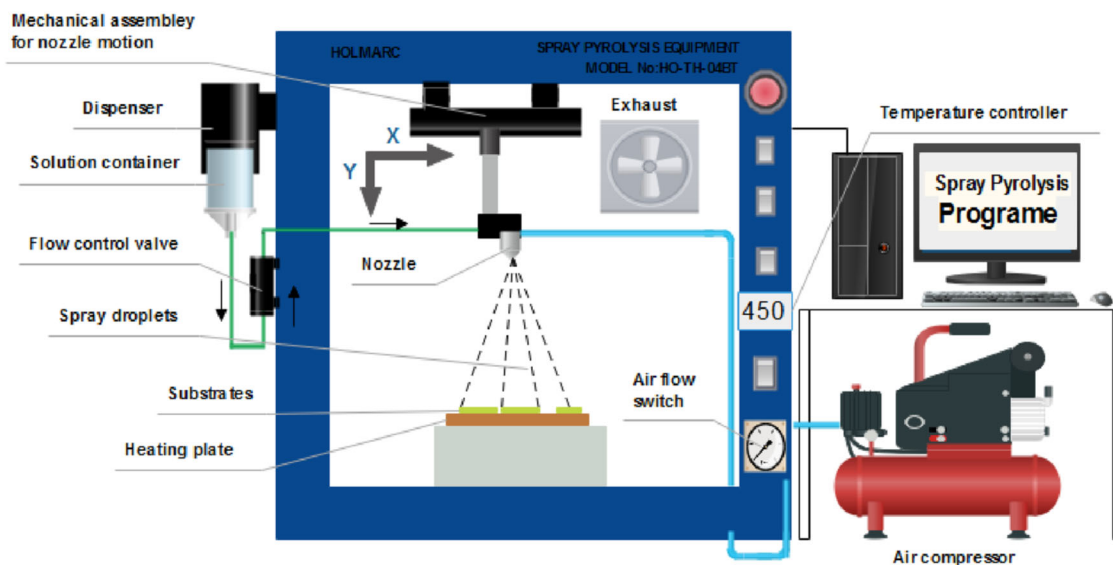
Fig. 1 Schematic diagram depicting the spray pyrolysis technique

2 Materials and methods

2.1 Materials

The synthesis of pristine ZnO and V-doped ZnO thin films is achieved by using commercial reagents. Zinc acetate dihydrate (Zn $(CH_3COO)_2.2H_2O$ 98%) and Vanadium (III) 2,4-pentanedionate ($C_{15}H_{21}O_6V$, 97% trace metals basis) were used as the host precursors.

2.2 Methods

Spray pyrolysis process grows thin film by spraying a precursor solution on a heated surface, where the chemical constituents react to form a chemical compound. The chemical reactants are selected such that the products other than the desired compound are volatile at the temperature of deposition. It is a relatively simple, scalable and efficient technique. A schematic view of the set-up used in our Lab is depicted in Fig. 1. A starting solution, including Zn precursors, is first sprayed by using a nozzle, assisted by a carrier gas, over a hot substrate. When the fine droplets reach the substrate, the solid compounds interact to become a novel chemical compound. ZnO thin films of different V-doping concentrations (0, 1, 2, 3 and 4 at.%) were deposited upon a borosilicate glass substrates of 2" × 2" at 450 °C. The concentration of this solution is 0.1 M. (Zn $(CH_3COO)_2.2H_2O$) was used as a precursor, which was prepared by dissolving in double-distilled water and methanol. The nozzle was set at a distance of 15 cm from the substrate. The solution flow rate was maintained constant at 1 ml/min. Air was used as the carrier gas, at the pressure of 1 bar. Deposition time was 2 min. Where aerosol droplets come near the substrates, a pyrolysis process occurs and highly adherent ZnO films are thus generated.

3 Characterization

The structural properties of the films were studied using Bruker D8 Advance X-ray diffractometer (USA) with Cu Ka radiation (λ 1.5418 Å) and instrument settings of 40 kV and 40 mA. The scan range was set from 3° to 100° with step size at 0.010°. The film morphology was studied using scanning electron microscopy (SEM) (FEI Quanta FEG 650 FE-SEM, USA) at 10 kV. The average compositions of the layers were determined by using elemental analyzer Bruker Quantax EDS (Hillsboro, Oregon, USA) installed in the same SEM system using an acceleration voltage of 15 kV. The chemical states of the constituent elements of films were investigated by X-ray photoelectron spectroscope (XPS) analysis system (Thermo Fisher ESCALAB 250i, Waltham, Massachusetts, USA). The surface roughness of the films was obtained using AFM equipment Bruker AXS Dimension Icon model, Fitchburg, WI, USA). A peak force quantitative nano-mechanical mapping mode in air was employed to acquire thin film roughness as well as the nano-mechanical and topographical images. NanoScope analysis software (Bruker, Fitchburg, WI, USA) was used to analyze AFM images to quantify membranes' roughness at scanning scale of 1 μm × 1 μm with a scanning rate of 0.751 Hz, peak force amplitude of 150 nm and frequency of 2 kHz. All AFM measurements were conducted using etched silicon probes (Bruker TESP-V2 AFM, Fitchburg, WI, USA). The method of TOF-SIMS based on the analysis of ionized sputtering products was

employed for depth profiling of the elemental composition of the samples. The optical transmittance spectra were performed in the wavelength range of 200–1100 nm using a UV-visible spectrophotometer (specord 210 plus). The hardness of the film was measured by using a Microhardness tester MHV-2000 with a Vickers Indenter. The MHV-2000 has a variable loading instrument ranging from 10 grams to 2000 grams. In our present study, we have used the test force 1.961 N (corresponding to 200 grams force) and a dwell time of 10 s to avoid any crack formation during indentation.

4 Results and discussions

4.1 Structural properties

The X-ray diffraction patterns of pristine ZnO and V-doped ZnO thin films conducted in the 2θ scan are shown in Fig. 2. Results revealed that all the grown films are polycrystalline in nature. No signal associated to zinc, vanadium, or their oxides were observed in the XRD pattern. The observed peaks are associated to (100), (002), (101), (102), (110), (103), and (112) orientations planes, thereby confirming the hexagonal wurtzite structure, and indicating that the structures of the V-doped ZnO are not changing after the incorporation of vanadium. The peak intensity of (100) peak is found to be increasing with V load while that of (002) and (101) peaks are decreasing. No distinct variation in the peak intensities of other higher 2θ peaks are observed. The overall integral intensity of all the crystalline phases were found to increase with V load. It could
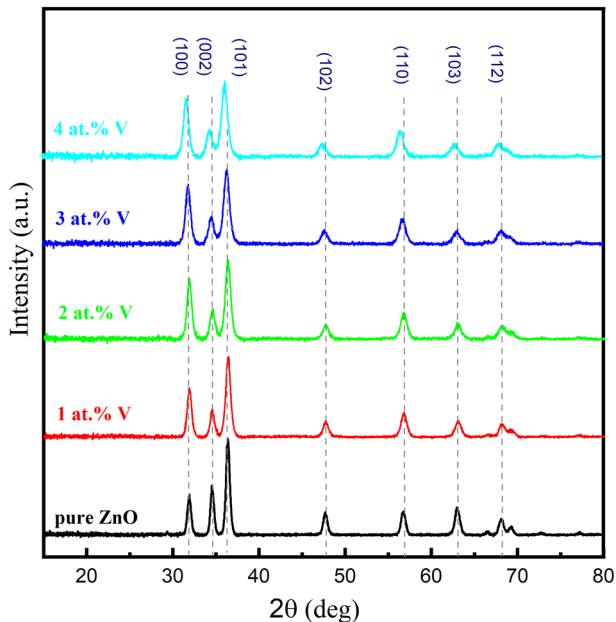
be possible that V promotes preferential growth along (100) at the expense of (002) and (101) phases. Further, the film with the (101) peak is a measure of the interplanar spacing for two neighboring layers of ZnO and its low intensity could, at first sight, be associated with the shielding effect of the reticular crystallographic plane (101) caused by the incorporation of Vanadium ions into ZnO matrix. This observed phenomenon is consistent with the results reported by Teng et al. [28]. In addition, vanadium may be a potential substitute Zn^{2+}(r 0.74 Å) [28] ions in different valence states and ionic radius [28], such as V^{5+} (r 0.54 Å) [29], V^{4+} (r 0.63 Å) [30], V^{3+} (r 0.74 Å) [31, 32], and V^{2+} (r 0.93 Å) [33]. This means that the difference in ionic radius between Zn and V is crucial to the change lattice parameters (either expanding or narrowing). In other words, vanadium ions which have a larger ionic radius than Zn^{2+} result in increased lattice parameters while substituting the zinc ions which have smaller ionic radius, and resulting though in decreased lattice parameters [31, 33]. The lattice constants a and c are calculated using the following formula [34]:

$$\frac{1}{d_{(hkl)}^2} = \frac{4}{3}\left[\frac{h^2 + hk + k^2}{a^2}\right] + \frac{l^2}{c^2} \tag{1}$$

The structural parameters of pristine ZnO and V-doped ZnO thin films are shown in Table 1.

4.2 Methodology for determining grain size and topography (AFM) analysis

We extract the features of grain size from AFM images by applying the self-correlation function G and the approach given in reference [35, 36] The function G of the self-correlation is given by the following equation [36]:

$$G(k_1, k_2) = \sum_{i=1}^{512} \sum_{j=1}^{512} h(i,j) \times h(i + k_1, j + k_2) \tag{2}$$

where $h(n, m)$ which is the height of the film at the point of coordinates (i, j).

Fig. 2 XRD patterns of pure ZnO and V-doped ZnO thin films with different V doping concentrations

Table 1 Lattice constants variation of pristine ZnO and V-doped ZnO thin films

Doping concentration (at.%)	2 theta	Lattice constants	
		a (Å)	c (Å)
0	34.56	3.237	5.1872
1	34.53	3.239	5.1907
2	34.53	3.243	5.1901
3	34.55	3.244	5.1877
4	34.55	3.246	5.1872

From a geometrical standpoint, the self-correlation function investigates the relationship between the original image and an image shifted from the original center by a distance k_1 and k_2. As a result, this function always achieves its maximum at the center. The shape of the maximum at the center of the 2D-correlation image provides access to the average shape of the deposits only in x-, and y-axis, and not in the z-axis

Figure 3 displays a typical example (1 at.% of V-doped ZnO films) of the mentioned procedure for determining grain size. We can provide two lengths (dx and dy) using cross-sections along x-axis (see Fig. 3C) and along y-axis (Fig. 3D), respectively. The length dx extracted in the x-axis is nearly the same as the length dy extracted in the y-axis, as illustrated in Fig. 3C, D. Thus, it may be said that the size of grain has a circular form with a mean diameter of d dx dy on the (x, y)-plane.

The AFM analysis of the pristine ZnO film reveals a relatively rough surface structure with randomly oriented grains and with sizes varying in 200–300 nm (A_0 in Fig. 4). These grain size values are much bigger than the average size of the crystallites as predicted by XRD. It can thus be concluded that such grains are formed by the clustering of many crystallites. The V-doping has found to be effective in improving the morphology of the films (see Fig. 4). The self-correlation function AFM images in Fig. 4 (C_0–C_4) shows clearly the increase of the grain size as well as the change in the grain shape by increasing the V content. Moreover, as indicated in Fig. 5b the root mean square (RMS) roughness of the V-doped ZnO thin films decreased with increasing the V concentration and leads to an improvement of the surface roughness. In line with these observations, similar trend has been reported by Kara et al. [37] and Amlouk et al. [38] for Mg-doped ZnO and Yb-doped ZnO thin films, respectively. Based on this analysis, the improvement of the surface roughness after introducing

vanadium into ZnO matrix may increase the electrical conductivity by providing more paths for electrons and thereby decreasing the electrical resistivity.

From self-correlation function images (1 μm × 1 μm) shown in Fig. 4 (C_0-C_4), it can be clearly seen that in the pristine ZnO, grain size seems to grow in a preferential direction. This preferential growth still dominant when the V-doping concentration is below 2 at.% (see Fig. 5a, Zone I). However, with increasing the V-doping up to 4 at.%, a significant decrease in the grain size elongation is observed in the favored y-axis. In fact, we reach values of dx that are substantially equivalent to those of dy (see Fig. 5a, Zone II). No preferential growth direction could be noticed for a V-doping above the 2 at.%.

4.3 Chemical composition analysis

4.3.1 X-ray photoelectron spectroscopy (XPS)

The XPS characterizations were performed to confirm the chemical composition and to ascertain the oxidation states in the films. Figure 6a shows the survey of the pristine ZnO and V-doped ZnO thin films with vanadium doping concentration of 0, 2 and 4 at.%. The scan was carried out within a binding energy range of 0–1400 eV. Photoelectron peaks of all the principal elements, Zn, O and V were clearly detected. Low intensity C1s peak is also observed, thereby confirming the presence of a carbon contamination in the films. The atomic concentrations (at.%) of the elements are estimated and tabulated in Table 2.

High resolution scans of Zn2p, O1s and V2p were performed to analyze the chemical states. Figure 6b–d illustrates the finely scanned core level binding energy curves of Zn-2p, O-1s and V-2p at 0, 2 and 4 at.% V-doped ZnO, respectively. The Zn-2p spectrum has two broadly resolved
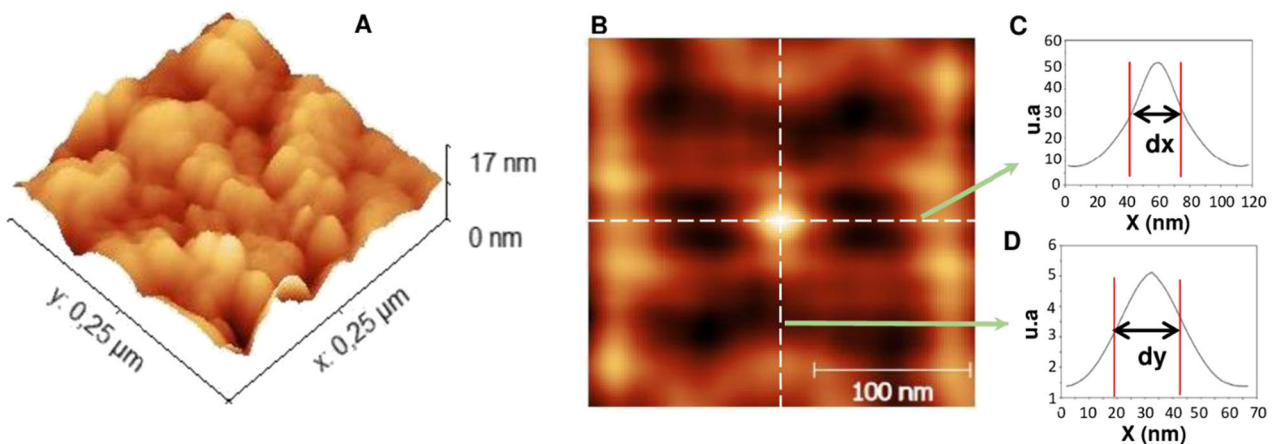
Fig. 3 A 3D AFM image (0.25 × 0.25) μm of the 1 at.% of V-doped ZnO films synthesized on glass (**B**) self-correlation function of image (**A**); **C** profile of the self-correlation function along line axis-x. dx is

the line width at half maximum of the central peak in this direction; **D** profile of the self-correlation function along axis-y. dy is the line width at half maximum of the central peak in the direction y
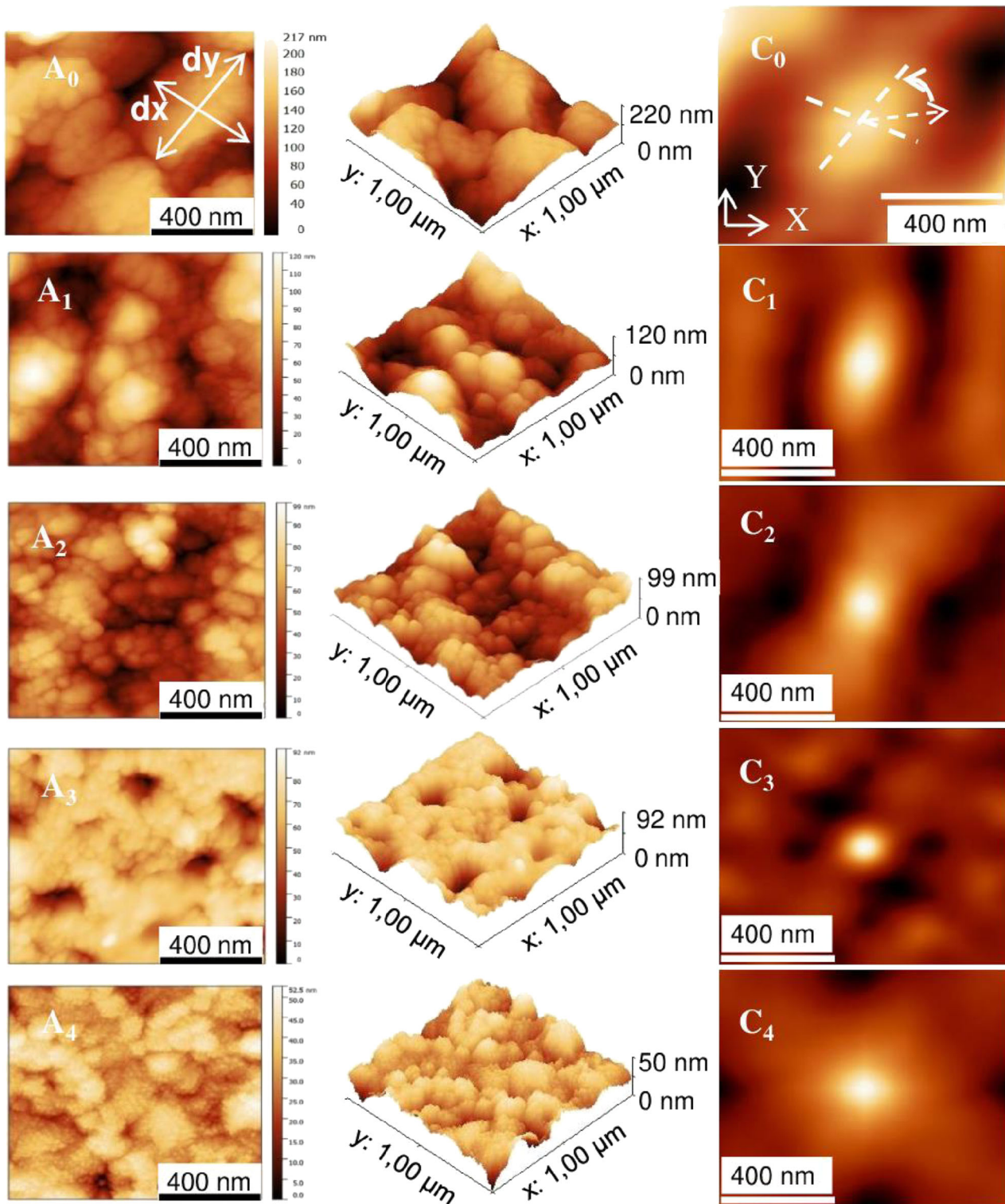
Fig. 4 Two, three-dimensional and self-correlation function AFM images of pure ZnO and V-doped ZnO thin films with different V doping concentrations. C_0, C_1, C_2, C_3 and C_4 are self-correlation function images calculated using respectively images A_0, A_1, A_2, A_3 and A_4 as input. C_0, C_1, C_2, C_3, and C_4 are zoomed images of the self-correlation function around the center peak to better depict the shape variations of the grain size

Fig. 5 **a** Grain size as function of vanadium concentrations at.%, **b** RMS roughness as a function of Vanadium concentrations. The dashed lines are guide to the eye
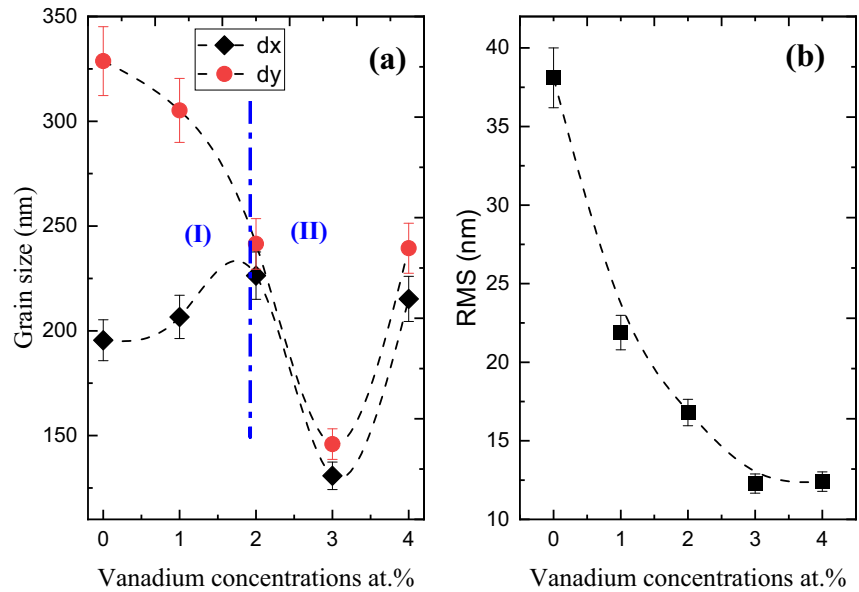
peaks at around 1021 and 1044 eV, with a spin-orbit splitting of (23.03 ± 0.02) eV between $2p_{1/2}$ and $2p_{3/2}$ peaks, irrespectively to the doping level. However, with increasing dopant concentrations, a slight blue shift is seen in both $2p_{1/2}$ and $2p_{3/2}$ features. The two peaks are symmetric and fit with a single Gaussian function each. The XPS data confirm that Zn exists only in $+2$ oxidation state in the films [39, 40].

The O1s peak profile shows an evident asymmetry which can only be deconvoluted by two Gaussian profiles, located at 530 and 531 eV (see Fig. 6c). This reflects the existence of two different forms of oxygen bonding present in the films. The more intense peak at 530 eV is attributed to O^{2-} ions in wurtzite ZnO structure while its left shoulder peak is related to O^{2-} ions originating from oxygen vacancies in the partially reduced regions within the ZnO matrix [41], or might be due to chemisorbed oxygen impurities [42]. These native defects, like oxygen vacancies, Zn interstitials, etc., enhance the electrical conductivity of ZnO films. The integral intensity of the peaks at ~531 eV increases with V-doping and is highly suggesting an increase of such native defect, which may lead to an enhancement of the electrical conductivity.

Figure 6d shows the high resolution XPS spectra of V-2p states present in the films. The spectrum consists only of $2p_{3/2}$ profile. Its high energy spin-orbit counterpart ($2p_{1/2}$) is within the error limits of the XPS profile and is thus overshadowed. This might be due to the low concentration of V in the films. The $2p_{3/2}$ peak profiles are asymmetrical and can be fitted using three Gaussian profiles. Due to the absence of $2p_{1/2}$ peak, the energy splitting of V 2p state cannot be determined. Thus, the oxidation states of the V in the films are predicted after comparing it with literature data.

After fitting the XPS spectra with Gaussian profile, it is observed that vanadium is present in mixed valence state of

V^{3+}, V^{4+} and V^{5+} in the films. Peak positions at 515.3 eV (2 at.%) and 515.3 eV (4 at.%) relates to V^{3+} state [43]. Peak positions at 516.4 eV (2 at.%) and 516.3 eV (4 at.%) attributes to the ions of the valence state V^{4+} [44, 45]. V^{5+} valence state exists at peak positions 517.3 (2 at. %) and 517.2 eV (4 at.%) V doped ZnO [46]. It is clearly observed that V^{5+} is found to be the most stable phase, with ~47% dominance, while V^{3+} (~30%) and V^{4+} (~23%) are oxygen deficient states. Also, V^{5+} phase growth increases (~55%) with increase in V-doping to 4 at.%. It is expected that V^{5+} state exists as a different phase outside the ZnO lattice and, therefore, does not contribute as a donor. Rather, they act as scattering centers for charge carriers which increases the film resistivity. Non-stoichiometric phase V^{2+} may also be present in the sample but beyond the reach of XPS detection as an active phase. The oxygen deficit V states may act as a donor and are helpful in the development of transparent conducting oxides.

Our XRD results confirm a lattice expansion which could be possible either due to inclusions of V—ion states with higher ionic radius, such as, V^{2+} in the lattice or due to residual stress in the films. Our XPS results ruled out the possibility of existence of V^{2+} valence state. So, the observed low angle shift of XRD peaks and thereby, the predicted lattice expansion is possible due to residual stress in the films.

### 4.3.2 Energy dispersive spectroscopy (EDS)

To quantify the presence of Zn, O, and V elements in films with high accuracy, the EDX analysis was performed. The atomic concentrations (at.%) of Zn, O and V elements in the films have been reported in Table 2. Based on EDX outcomes, Zn, O and V contents agreed well with the XPS data. The formation of ZnO and the presence of the V-dopant in the film
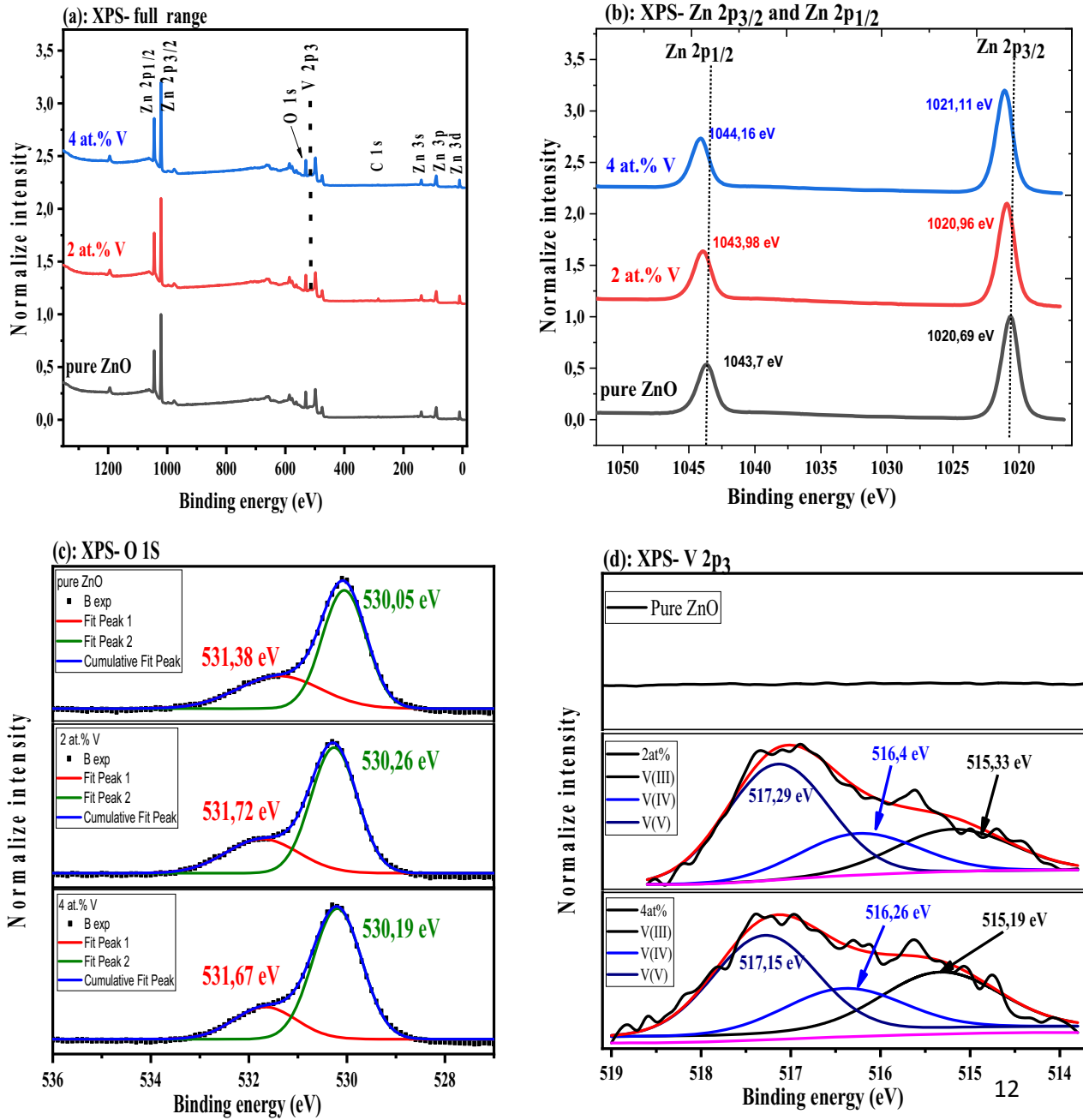
Fig. 6 a The full-range XPS spectrum of pure ZnO and V-doped ZnO thin films with V-content of 0, 2 and 4 at.%, **b–d**: the good resolution photoemission spectrum of Zn-2p, O-1s and V-2p respectively

Table 2 The composition of ZnO films doped with different V doping concentrations was obtained by EDX and XPS

Doping concentration (at.%)	EDX (at.%)				XPS (at.%)			
	O	Zn	V	C	O	Zn	V	C
0	46.27	15.26	/	3.88	47.33	46.54	/	6.12
1	42.58	46.35	0.55	8.54	/	/	/	/
2	42.22	37.3	1.06	9.58	42.33	41	1.39	15.28
3	42.12	36.9	1.52	10.1	/	/	/	/
4	41.24	42.71	2.22	11.9	46.69	45.74	2.66	4.91
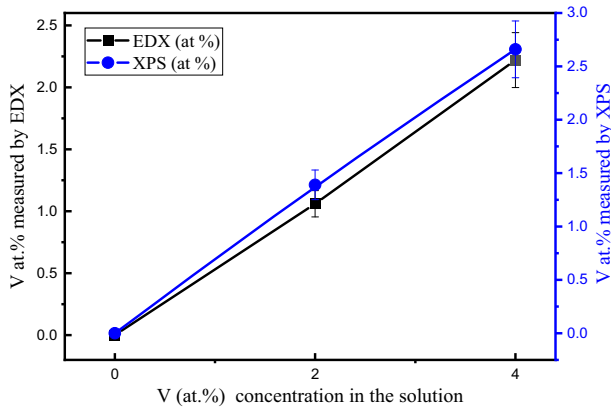
Fig. 7 Relative V content measured with EDX and XPS as function of V content within solution

with the expected stoichiometry (nearly the same proportion of Zn and O in the films) was confirmed using the two complementary techniques. Figure 7 shows the V concentration in atomic percent (at.%) within the films as determined directly from the EDS software (i.e., Esprit 1.9) after performing the routine quantitative verification and calibration of the system. Figure 7 shows the relative V content measured with EDX and XPS as function of V content. An accurate control of V content is thus achievable.

4.3.3 Time-of-flight secondary ion mass spectroscopy (TOF-SIMS)

Usually the TOF-SIMS approach was used to determine the spatial distribution of different chemical elements with depth across and interfaces of the films. This method is regarded as a very powerful and surface-sensitive one. In the current study, depth profiling was carried out using IONTOF TOF-SIMS5 model to analyze deposited thin films and detect associated species throughout the thickness. Primary analysis was performed by positive Bi+ ion beam at 30 keV and ~1.29 pA current over a $100 \times 100\ \mu m^2$ analyzed area using sawtooth rastering mode. The depth profile has been conducted in positive polarity which targets the positive ions with secondary sputtering source.

Figure 8 shows a representative TOF-SIMS spectra performed on pristine ZnO (Fig. 8a) along with the V-doped films at concentrations 1, 2, 3 and 4 at.% (Fig. 8b–e, respectively), deposited onto Si substrate. In Fig. 8a, SIMS spectra shows perfect signals of Zn and O, constant throughout the film thickness. We notice also the presence of carbon signal which decreases exponentially with respect to the sputtering time (i.e., as a function of the film thickness) and is undoubtedly associated to the C contamination present onto the ZnO surface. Figure 8b–e shows clear Zn, O signals as well (along with C contamination) as evidence of the successful V-doping. The latter (i.e., V) is looking

constant throughout the film thickness regardless to its concentration. All profiles (Zn, O and V) are found quite similar in shape, in the sense that all signals related to ZnO and V doped ZnO layers (namely, Zn, O and V) are quite constant (except that related to carbon contamination).

One should note that SIMS measurements are not employed as quantitative analyses, the intensities of the species are intimately impacted by the sputtering time, however, Zn and O depth profiles are found to be clearly much more intense than that of the V doping signals. In sum, TOF-SIMS analysis confirmed the existence of all the deposited species and the successful constant-doping with vanadium throughout the entire film thickness.

4.4 Optical properties (UV-Vis-NIR)

The transmittance spectra of our films were measured by a UV-Vis spectrophotometer in the 200–1000 nm range and results are displayed in Fig. 9. It can be seen that the transmittance (T%) of the films increases with increasing vanadium concentration. No oscillations in the spectra were observed reveals absence of the optical interferences on the surface [47]. The spectra also show a sharp absorption edge located at 376.5 nm, which confirms the crystal quality of our grown films as amorphous films do not show any sharp absorption edges [48].This observation corroborates well with our XRD analysis.

Sudden decrease in T% below 450 nm denotes absorption edge due to ZnO. The band edge of the pristine ZnO film can be seen ~370 nm. However, with increasing V concentration, the band edges shift toward lower wavelength thereby leading to a change in the band gaps. This is owing to the V-doping, also known as the Burstein–Moss shift.

The band gap (Eg) of both type of thin films (pristine ZnO and V-doped films) were estimated from the transmittance spectra of the absorption edge using Tauc relation [49] for a direct band gap semiconductor, using Eq. (3):

$$\alpha h\upsilon = A(h\upsilon - E_g)^{1/2} \tag{3}$$

where α is the absorption coefficient (cm^{-1}), h is Plank's constant (J-s), υ is the frequency of radiation (Hz), A is an appropriate constant and Eg is the band gap (eV).

Figure 9b reveals that the optical band gaps of the ZnO films increase from 3.18 to 3.26 eV with V-doping. However, the trend is not clear. According to Tauc plots, the band gap shows blue shift for lower doping concentrations (<3 at.%) and decreases for doping levels (>3 at.%). The increase in band gaps can be attributed to Burstein–Moss shift. Such a shift arises due to occupying lower conduction levels by the free charge carriers and thus, the valence electrons need more energy to go to the conduction band. This is reflected by the blue shift of electronic transition
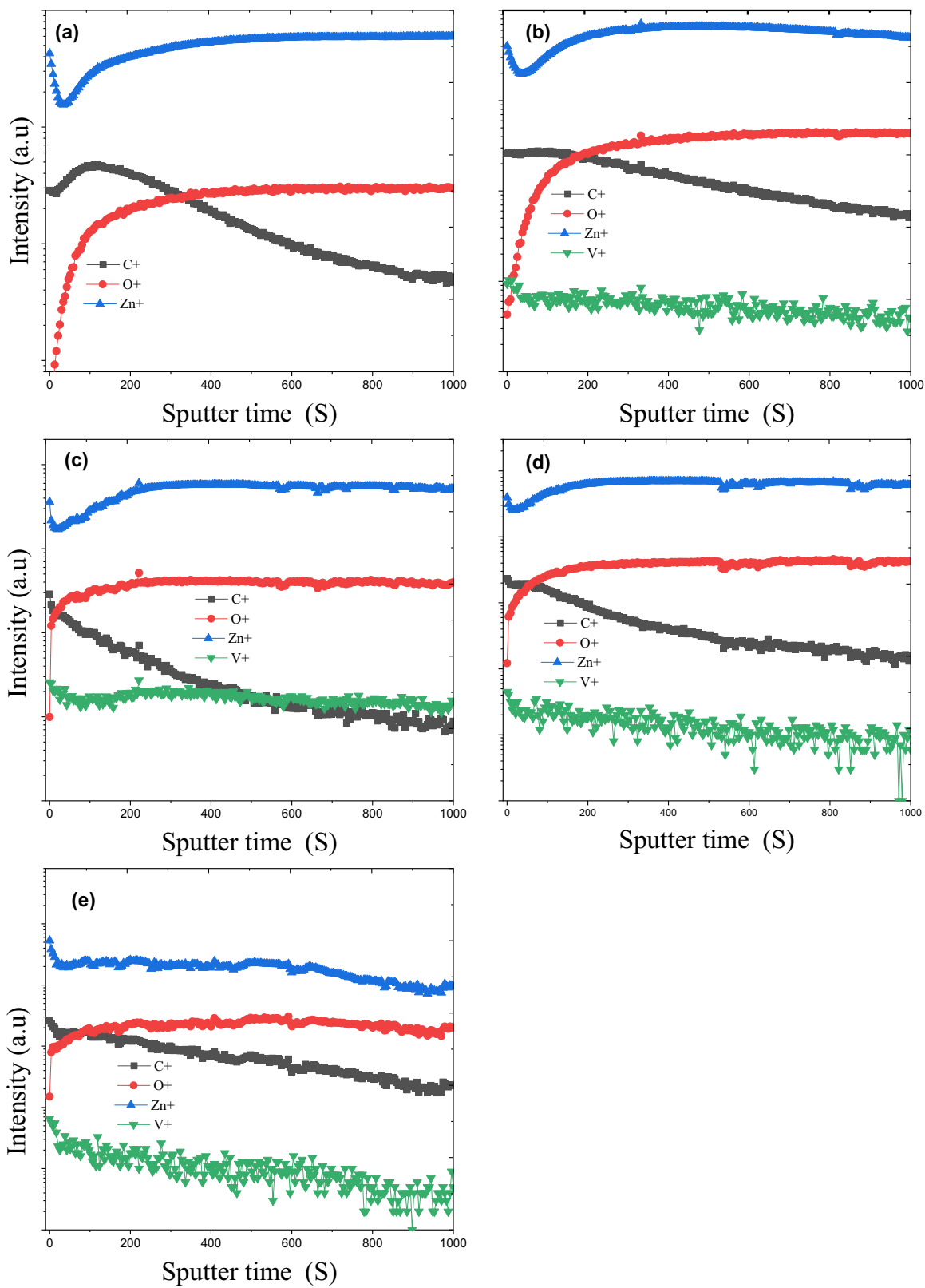
Fig. 8 Typical TOF-SIMS depth profiling of the **a** ZnO and ZnO doped Vanadium, **b** 1 at.%, **c** 2 at.%, **d** 3 at.% and **e** 4 at.%
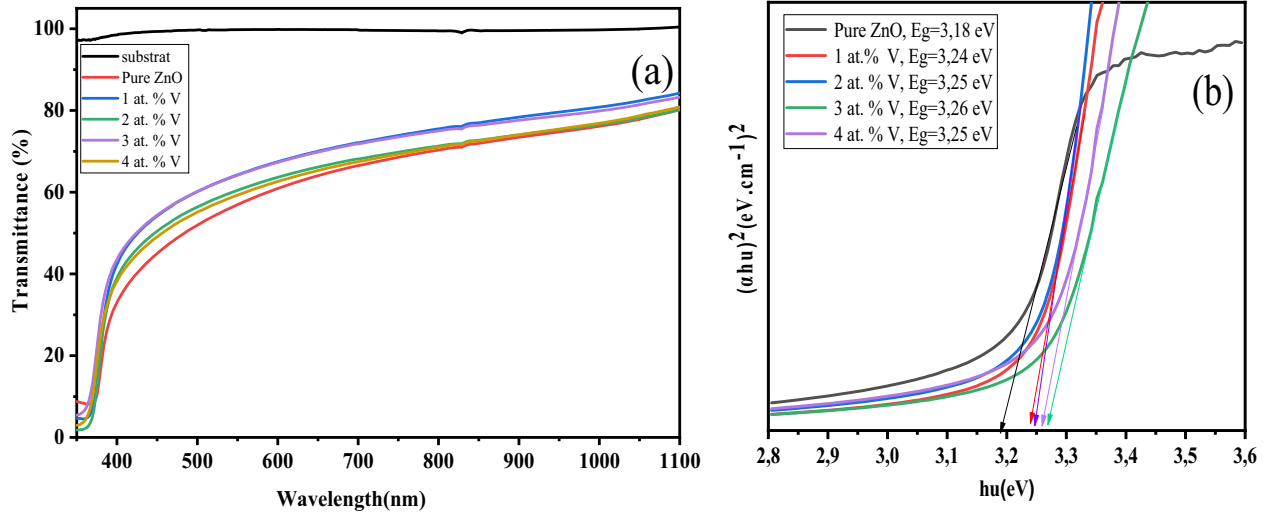
Fig. 9 **a** Transmission spectrum of pure ZnO and V doped ZnO thin films with different V doping concentrations. **b** The Optical band gap of pure ZnO and V doped ZnO films. The solid lines indicate the fit of the optical band gap energy

frequencies in the UV–Vis spectra. the Fermi energy state move toward the conduction band, broadening the optical band gap [50]. A red shift in band gap beyond 3 at.% doping may appear due to an increase in defects and impurities, as well as a complete lack of dopant substitution by host atoms or interstitials. This can change the Fermi energy state by lifting the valence band maximum and lowering the conduction band minimum leading to band gap reduction [51]. Besides, as mentioned previously by other reports the optical band gap reduction could be influenced by a variety of variables such as carrier concentration, grain size, or stoichiometry, as well as variations in lattice strain [52–54].

Although, the optical properties predict some increase in carrier concentration with V load, its relative change in mobility is not clear from these optical results. Systematic Hall effect measurements can only confirm whether these films have charge carrier mobility high enough to be considered for the fabrication of p-n junctions or not.

4.5 Mechanical properties

The mechanical study was carried out through micro-indentation analysis using a conventional diamond-pyramidal-indenter Vickers test. Figure 10 depicts the obtained results. It is clear from this figure that the presence of V as dopants in ZnO films influenced its microhardness. To understand the relationship between (RMS) roughness and microhardness of these films, the (RMS) and Vickers Hardness (Hv) values of pure and V-doped ZnO films were plotted as a function of different V doping concentrations, shown in Fig. 10. The graph shows that by increasing V concentration, the microhardness increases in the range
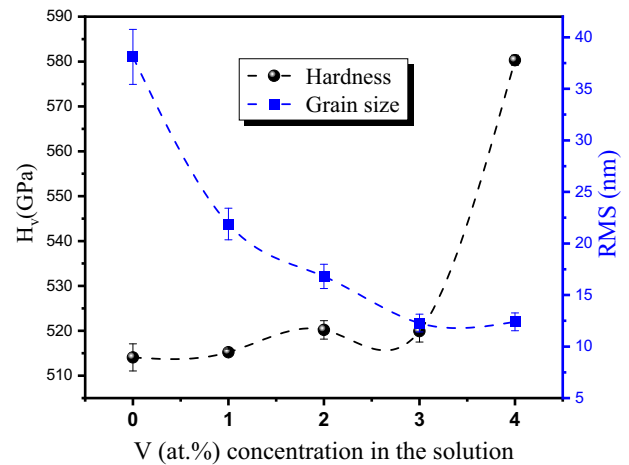
Fig. 10 Vickers hardness and root mean square (RMS) of pure ZnO and V-doped ZnO thin films with different V doping concentrations. The dashed lines are guide to the eye

514–580 GPa. Each data point is the average of three Vickers measurements and the error bars are the standard deviations.

It can be assumed that these changes could be explained by the RMS roughness variation as well as by the possible change on the crystal lattice caused by the incorporation of V atoms. Indeed, the decrease of roughness seen in AFM results can explain the increase on microhardness values. Similar observation has been reported by Amlouk et al. [38], where they showed an enhancement in the surface roughness and an increase in microhardness of their ytterbium-doped ZnO thin films system. According to these conducted mechanical analysis, the spray coated V-doped ZnO thin films on glass substrate are a suitable candidate for usage as light window and/or transparent conducting oxides

in plenty of optoelectronic devices that are requiring high mechanical properties.

5 Summary

Pristine ZnO and V-doped ZnO thin films were successfully grown by the chemical spray pyrolysis technique by varying the V-dopant concentration in the range 0–4 at.% at a constant substrate temperature of 450 °C. XRD measurements revealed that the V-doped ZnO films are polycrystalline structure belonging to the ZnO hexagonal wurtzite type with a dominant orientation along (101) direction. The surface roughness of the films changed with respect to the V concentration. The result of EDS and XPS analyses showed that the V was successfully incorporated into the lattice of ZnO by a mixed state of +3, +4 and +5. The average optical transmittance of all films was approximately between 60 and 80% above the fundamental absorption edge. The TOF-SIMS analysis confirmed the presence of all the deposited elements over the surface, as well as the successful constant-doping with vanadium over the entire film thickness. The energy band gap values vary between 3.18 and 3.26 eV with the change in V concentration. The mechanical tests show that V doped ZnO synthesized via a spray technique is appropriate for application in a wide range of optoelectronic devices.

Compliance with ethical standards

Conflict of interest The authors declare no competing interests.

Publisher's note Springer Nature remains neutral with regard to jurisdictional claims in published maps and institutional affiliations.

References

1. Chen Y, Bagnall D, Yao T (2000) ZnO as a novel photonic material for the UV region. Mater Sci Eng: B 75:190–198
2. Minami T, Ida S, Miyata T (2002) High rate deposition of transparent conducting oxide thin films by vacuum arc plasma evaporation. Thin Solid Films 416:92–96
3. Look DC, Hemsky JW, Sizelove J (1999) Residual native shallow donor in ZnO. Phys Rev Lett 82:2552
4. Oba F, Togo A, Tanaka I, Paier J, Kresse G (2008) Defect energetics in ZnO: A hybrid Hartree-Fock density functional study. Phys Rev B 77:245202
5. Nebatti A, Pflitsch C, Atakan B (2017) Unusual application of aluminium-doped ZnO thin film developed by metalorganic chemical vapour deposition for surface temperature sensor. Thin Solid Films 636:532–536
6. Ellmer K, Klein A, Rech B (2008) Transparent Conductive Zinc Oxide: Basics and Applications in Thin Film Solar Cells. Springer Series in Materials Science, vol 104, Springer, Berlin
7. Granqvist CG (2007) Transparent conductors as solar energy materials: A panoramic review. Sol energy Mater Sol cells 91:1529–1598
8. Aïssa B, Khakani El MA (2009) The channel length effect on the electrical performance of suspended-single-wall-carbon-nanotubes-based field effect transistors. Nanotechnology 20:175203. https://doi.org/10.1088/0957-4484/20/17/175203
9. Özgür Ü, Hofstetter D, Morkoc H (2010) ZnO devices and applications: a review of current status and future prospects. Proc IEEE 98:1255–1268
10. Ellmer K (2000) Magnetron sputtering of transparent conductive zinc oxide: relation between the sputtering parameters and the electronic properties. J Phys D: Appl Phys 33:R17
11. Minami T (2000) New n-type transparent conducting oxides. MRS Bull 25:38–44
12. Özgür Ü, Alivov YI, Liu C, Teke A, Reshchikov M, Doğan S, Avrutin V, Cho S-J (2005) Morkoç, A comprehensive review of ZnO materials and devices. J Appl Phys 98:11
13. Minami T, Suzuki S, Miyata T (2001) Transparent conducting impurity-co-doped ZnO: Al thin films prepared by magnetron sputtering. Thin Solid Films 398:53–58
14. El Mir L, Ghribi F, Hajiri M, Ayadi ZB, Djessas K, Cubukcu M, von Bardeleben H (2011) Multifunctional ZnO: V thin films deposited by rf-magnetron sputtering from aerogel nanopowder target material. Thin Solid Films 519:5787–5791
15. Ko SH, Lee D, Kang HW, Nam KH, Yeo JY, Hong SJ, Grigoropoulos CP, Sung HJ (2011) Nanoforest of hydrothermally grown hierarchical ZnO nanowires for a high efficiency dye-sensitized solar cell. Nano Lett 11:666–671
16. Ryu Y, Lee T, Lubguban J, White H, Park Y, Youn C (2005) ZnO devices: Photodiodes and p-type field-effect transistors. Appl Phys Lett 87:153504
17. Peng W, He Y, Wen C, Ma K (2012) Surface acoustic wave ultraviolet detector based on zinc oxide nanowire sensing layer. Sens Actuators A: Phys 184:34–40
18. Law J, Thong J (2006) Simple fabrication of a ZnO nanowire photodetector with a fast photoresponse time. Appl Phys Lett 88:133114
19. Yousefi R, Jamali-Sheini F, Cheraghizade M, Khosravi-Gandomani S, Sáaedi A, Huang NM, Basirun WJ, Azarang M (2015) Enhanced visible-light photocatalytic activity of strontium-doped zinc oxide nanoparticles. Mater Sci Semiconductor Process 32:152–159
20. Tarwal N, Rajgure A, Patil J, Khandekar M, Suryavanshi S, Patil P, Gang M, Kim J, Jang J (2013) A selective ethanol gas sensor based on spray-derived Ag–ZnO thin films. J Mater Sci 48:7274–7282
21. Chen J, Wang J, Zhang F, Zhang G, Wu Z, Yan P (2008) The effect of La doping concentration on the properties of zinc oxide films prepared by the sol–gel method. J Cryst Growth 310:2627–2632
22. Xu L, Xiao S, Zhang C, Zheng G, Su J, Zhao L, Wang J (2014) Optical and structural properties of Sr-doped ZnO thin films. Mater Chem Phys 148:720–726
23. Nebatti Ech Chergui A, Pflitsch C, Atakan B (2021) Atmospheric pressure metal-organic chemical vapor deposition (AP-MOCVD) growth of undoped and aluminium-doped ZnO thin film using hot wall reactor. Surf Interfaces 22:100883
24. Kadaria AS, Ech-Chergui AN, Mohamedi MW, Zoukel A, Sabrina T, Mehdi A, Driss-Khodja K, Amrani B (2009) Microcontroller-Based Moving Message Display Powered by Photovoltaic Energy. Ain Shams Journal of Electrical Engineering (ASJEE) 2:15–25

25. Nebatti AE, Pflitsch C, Eckert C, Atakan B (2019) Rapid Thermal (RT) MOCVD of Undoped and Al Doped ZnO Thin Films. ECS Trans 25:459–465

26. Minkov D (1989) Calculation of the optical constants of a thin layer upon a transparent substrate from the reflection spectrum. J Phys D: Appl Phys 22:1157

27. Menaka SM, Umadevi G, Manickam M (2017) Effect of copper concentration on the physical properties of copper doped NiO thin films deposited by spray pyrolysis. Mater Chem Phys 191:181–187

28. Li-Wei W, Zheng X, Li-Jian M, Teixeira V, Shi-Geng S, Xu-Rong X (2009) Influence of concentration of vanadium in zinc oxide on structural and optical properties with lower concentration. Chin Phys Lett 26:077801

29. Yang Y, Song C, Zeng F, Pan F, Xie Y, Liu T (2007) V 5+ ionic displacement induced ferroelectric behavior in V-doped ZnO films. Appl Phys Lett 90:242903

30. Çolak H, Türkoğlu O (2012) Structural and electrical properties of V-doped ZnO prepared by the solid state reaction. J Mater Sci: Mater Electron 23:1750–1758

31. Olive-Méndez SF, Santillán-Rodríguez CR, González-Valenzuela RA, Espinosa-Magaña F, Matutes-Aquino JA (2014) Role of vanadium ions, oxygen vacancies, and interstitial zinc in room temperature ferromagnetism on ZnO-V 2 O 5 nanoparticles. Nanoscale Res Lett 9:1–7

32. Wen-Chen Z, Shao-Yi W, Hui-Ning D, Jian Z (2002) Studies of electron paramagnetic resonance parameters and defect structures for Ti2+ and V3+ ions in CdS crystals. Spectrochimica Acta Part A: Mol Biomolecular Spectrosc 58:537–541

33. Akilan T, Srinivasan N, Saravanan R, Chowdury P (2014) Structure of Vanadium-Doped Zinc Oxide, Zn1–XV x O. Mater Manuf Process 29:780–788

34. Cullity B, Stock S (2001) Elements of x-ray diffraction. Prentice Hall, Upper Saddle River, NJ, p 388

35. Bubendorff J, Garreau G, Zabrocki S, Berling D, Jaafar R, Hajjar S, Mehdaoui A, Pirri C (2009) Nanostructuring of Fe films by oblique incidence deposition on a FeSi2 template onto Si (1 1 1): Growth, morphology, structure and faceting. Surf Sci 603:373–379

36. Mechehoud F, Benaioun N, Hakiki N, Khelil A, Simon L, Bubendorff J-L (2018) Thermally oxidized Inconel 600 and 690 nickel-based alloys characterizations by combination of global photoelectrochemistry and local near-field microscopy techniques (STM, STS, AFM, SKPFM). Appl Surf Sci 433:66–75

37. Kara R, Mentar L, Azizi A (2020) Synthesis and characterization of Mg-doped ZnO thin-films electrochemically grown on FTO substrates for optoelectronic applications. RSC Adv 10:40467–40479

38. Amlouk A, Boubaker K, Amlouk M, Bouhafs M (2009) Study of ytterbium doping effects on structural, mechanical and opto-thermal properties of sprayed ZnO thin films using the Boubaker Polynomials Expansion Scheme (BPES). J Alloy Compd 485:887–891

39. Parmar NS, Choi J-W, Boatner LA, McCluskey MD, Lynn KG (2017) Formation of high concentrations of isolated Zn vacancies and evidence for their acceptor levels in ZnO. J Alloy Compd 729:1031–1037

40. Briggs D (1981) Handbook of X-ray Photoelectron Spectroscopy Wanger CD, Riggs WM, Davis LE, Moulder JF and Muilenberg GE (eds.) Perkin-Elmer Corp., Physical Electronics Division, Eden Prairie, Minnesota, USA, 1979. 190 pp. $195, in, Wiley Online Library

41. Tian X, Pan Z, Zhang H, Fan H, Zeng X, Xiao C, Hu G, Wei Z (2013) Growth and characterization of the Al-doped and Al–Sn co-doped ZnO nanostructures. Ceram Int 39:6497–6502

42. Ye Z, Wang T, Wu S, Ji X, Zhang Q (2017) Na-doped ZnO nanorods fabricated by chemical vapor deposition and their optoelectrical properties. J Alloy Compd 690:189–194

43. Alov N, Kutsko D, Spirovova I, Bastl Z (2006) XPS study of vanadium surface oxidation by oxygen ion bombardment. Surf Sci 600:1628–1631

44. Cornaglia L, Lombardo E (1995) XPS studies of the surface oxidation states on vanadium-phosphorus-oxygen (VPO) equilibrated catalysts. Appl Catal A: Gen 127:125–138

45. Silversmit G, Depla D, Poelman H, Marin G, De R (2006) Gryse, A fit procedure to determine the mean vanadium oxidation state from V2p phtotelectron spectra. BELVAC NEWS 22:3–8

46. Suchorski Y, Rihko-Struckmann L, Klose F, Ye Y, Alandjiyska M, Sundmacher K, Weiss H (2005) Evolution of oxidation states in vanadium-based catalysts under conventional XPS conditions. Appl Surf Sci 249:231–237

47. Nebatti A, Pflitsch C, Curdts B, Atakan B (2015) Using the acetylacetonates of zinc and aluminium for the Metalorganic Chemical Vapour Deposition of aluminium doped zinc oxide films. Mater Sci Semiconductor Process 39:467–475

48. Al Asmar R, Atanas JP, Ajaka M, Zaatar Y, Ferblantier G, Sauvajol JL, Jabbour J, Juillaget S, Foucaran A (2005) Characterization and Raman investigations on high-quality ZnO thin films fabricated by reactive electron beam evaporation technique. J Cryst Growth 279:394–402

49. O'Leary SK, Lim P (1997) On determining the optical gap associated with an amorphous semiconductor: A generalization of the Tauc model. Solid State Commun 104:17–21

50. Ameen S, Akhtar MS, Seo H-K, Kim YS, Shin HS (2012) Influence of Sn doping on ZnO nanostructures from nanoparticles to spindle shape and their photoelectrochemical properties for dye sensitized solar cells. Chem Eng J 187:351–356

51. Srinivasulu T, Saritha K, Reddy KR (2017) Synthesis and characterization of Fe-doped ZnO thin films deposited by chemical spray pyrolysis. Mod Electron Mater 3:76–85

52. Lee Y, Lee W, Kwon Y, Yeom G, Yoon J (1999) Effects of CdS substrates on the physical properties of polycrystalline CdTe Films. Thin solid films 341:172–175

53. Bentouaf A, Mebsout R, Rached H, Amari S, Reshak AH, Aïssa B (2016) Theoretical investigation of the structural, electronic, magnetic and elastic properties of binary cubic C15-Laves phases TbX2(X = Co and Fe). J Alloys and compounds 689:885–893. https://doi.org/10.1016/j.jallcom.2016.08.046

54. Yakuphanoglu F, Caglar Y, Ilican S, Caglar M (2007) The effects of fluorine on the structural, surface morphology and optical properties of ZnO thin films. Phys B: Condens Matter 394:86–92